

1 METHODS AND CODES FOR RESERVOIR–ATMOSPHERE ¹⁴C AGE 2 OFFSET CALCULATIONS

3

4 **Guillaume SOULET^{1,*}**5 1 Woods Hole Oceanographic Institution, Geology and Geophysics department, 266 Woods Hole Road, Woods
6 Hole, MA-02543, USA7 *corresponding author: gsoulet@whoi.edu8 **Abstract**

9 Reservoir age ¹⁴C offsets are invaluable tracers for past changes in carbon cycle and oceanic
10 circulation. Reconstruction of reservoir age offsets with time is also required for calibration
11 purposes (reconstruction of atmospheric calibration curve, calibration of non-atmospheric
12 radiocarbon ages). Thus, properly propagating the various uncertainties linked to reservoir age
13 offset is important for proper interpretation. However, approaches for reservoir age offset
14 calculation – especially when considering pairs of reservoir-derived ¹⁴C and calendar ages – are
15 usually not detailed and inadequate for proper propagation of uncertainties. Here, the various
16 ways to properly calculate reservoir age offsets are described with an emphasis on a new
17 approach when considering pairs of ¹⁴C and calendar ages. This approach maps the calendar age
18 distribution onto the ¹⁴C time scale prior to reservoir age offset calculation – the “*uncalibration-*
19 *convolution process*”. R codes computing reservoir age offsets based on available data are
20 presented. Finally, a case study focusing on the reconstruction of the speleothem-atmosphere ¹⁴C
21 age offsets of speleothem ¹⁴C data used in the latest release of the atmospheric calibration curve
22 is discussed.

23 **Keywords:** Reservoir age, reservoir effect, dead carbon fraction, radiocarbon modelling,
24 calibration curve, uncalibration process

25 **1. Introduction**

26 Reservoir age offset is a fundamental metric to study the dynamics of carbon exchanges between
27 the Earth's reservoirs and attendant impacts on past climate changes. It is also widely used in
28 geochronology calibration purposes. Whereas reservoir-atmospheric ^{14}C age offsets arise from
29 various natural and anthropogenic processes (for a review, see Jull et al., 2013), they always
30 derive from a $^{14}\text{C}/^{12}\text{C}$ disequilibrium between the considered carbon reservoir (e.g. surface or
31 deep ocean, freshwater systems, soil) and the contemporaneous atmosphere (i.e. the atmospheric
32 carbon reservoir). From a ^{14}C age point of view, this can be expressed as:

$$33 \quad d^{14}R(\theta) = \rho_{res}(\theta) - \rho_{atm}(\theta) \quad (1)$$

34 Equation (1) indicates that the reservoir age offset is the deviation $d^{14}R$ between the ^{14}C age of
35 the considered carbon reservoir ρ_{res} and the ^{14}C age of the contemporaneous atmospheric carbon
36 reservoir ρ_{atm} at a given calendar time θ . Therefore, an either perfect or imperfect estimate of
37 the calendar age θ needs to be available in order to derive the reservoir age offset. Note that the
38 atmospheric carbon reservoir is used as the reference when computing the reservoir age offset, as
39 it is the sole carbon reservoir in which ^{14}C is renewed and spatially uniform besides some second
40 order differences between hemispheres (Hogg et al., 2013). In addition, the atmospheric ^{14}C
41 concentration is quite precisely known for the past 14,000 calendar years and reasonably well
42 known back to 50,000 calendar years ago (Reimer et al., 2013). Consequently, it is possible to
43 reconstruct reservoir age offsets for calendar ages back to year 50,000 before the present (i.e.,
44 years before AD 1950; thereafter cal. a. BP). Moreover, equation (1) indicates that the reservoir
45 age offset must be quoted in “ ^{14}C years”.

46 Calculating reservoir age offsets seems straightforward. However, sometimes the calendar age θ
47 is necessarily weakly known, i.e. that an uncertainty is associated to it. Indeed it may have been

48 obtained through scientific measurements [e.g. U/Th dating (e.g. Druffel et al., 2008; Hall et al.,
49 2010; Southon et al., 2012) or tuning processes with calendrically-dated series of reference (e.g.
50 Heaton et al., 2013; Soulet et al., 2011a; Thornalley et al., 2011)]. In that case, mapping the
51 calendar age distribution onto the radiocarbon time scale (hereafter called “uncalibration”) is
52 required in order to get access to the atmospheric ^{14}C age corresponding to the calendar age
53 $\theta \pm \sigma_\theta$. The “uncalibrating” approach is sometimes vaguely detailed in the literature, e.g.,
54 Reimer et al. (2013) wrote: “*reservoir ages were calculated from the ^{14}C difference of the*
55 *overlap with the tree rings*”. After the “uncalibration” step, some authors propagated
56 uncertainties on the ^{14}C reservoir age offset through the use of the quadratic sum (e.g. Hall et al.,
57 2010). Even though this method produces an estimate of the reservoir age offset, it turns out to
58 be distributed according to a Gaussian distribution, since the approach neglects the structures of
59 the atmospheric calibration curve. When the atmospheric ^{14}C wiggles are taken into account, the
60 estimates of both “uncalibrated” ages and the resulting reservoir age offsets can be distributed
61 according to multi-modal and asymmetric probability distributions.

62 Properly propagating the various uncertainties linked to reservoir age offset may help for their
63 proper use and interpretation. This paper is intended to describe the various ways to calculate
64 reservoir age offsets with a focus on a Bayesian approach – the “*uncalibration-convolution*
65 *process*” – which properly propagates uncertainties linked to the reservoir-derived ^{14}C age, a
66 weakly *a priori* known calendar age and the atmospheric calibration curve. A case study
67 discusses the speleothem-atmosphere ^{14}C age offsets of speleothem ^{14}C data used in the latest
68 release of the atmospheric calibration curve. Free and open-source codes for proper reservoir age
69 offset calculations are provided.

70

71 **2. Reservoir age offset calculations and open-source codes**

72 According to equation (1), both the ^{14}C age of the considered reservoir (e.g. ocean, a lake, a soil)
73 and the ^{14}C age of the atmosphere in the calendar year θ have to be known to calculate the
74 reservoir age offset. Furthermore, whatever the information we have about calendar year θ –
75 perfectly known, weakly known or not known *a priori* – we must be certain that it corresponds to
76 the same event Y at which reservoir/atmosphere-derived objects ceased to incorporate carbon.
77 Hence, equation (1) can be written slightly differently:

$$78 \quad d^{14}R(Y) = \rho_{res}(Y) - \rho_{atm}(Y) \quad (2)$$

79 which says that the reservoir age offset at the calendar year θ of event Y [$d^{14}R(Y)$] is equal to the
80 difference between ^{14}C ages of the considered reservoir-derived and atmosphere-derived objects
81 that ceased to incorporate carbon at the calendar year θ of event Y ($\rho_{res}(Y)$ and $\rho_{atm}(Y)$,
82 respectively). From that statement, three cases of study are possible.

83

84 **2.1. Reservoir age offset calculation based on a pair of ^{14}C ages**

85 In that specific case both ^{14}C ages derived from the considered reservoir $\rho_{res}(Y) \pm \sigma_{\rho_{res}(Y)}$ and
86 from the contemporaneous atmosphere $\rho_{atm}(Y) \pm \sigma_{\rho_{atm}(Y)}$ are *a priori* known, whereas the
87 calendar year θ , corresponding to event Y , is unknown. The ^{14}C reservoir age offset $d^{14}R(Y)$ is
88 easily calculated according equation (2), and resulting uncertainty is given by:

$$89 \quad \sigma_{d^{14}R(Y)} = \sqrt{\sigma_{\rho_{res}(Y)}^2 + \sigma_{\rho_{atm}(Y)}^2} \quad (3)$$

90 Finally, the calendar year θ at which event Y occurred can be obtained by calibrating the
91 atmosphere-derived ^{14}C age $\rho_{atm}(Y) \pm \sigma_{\rho_{atm}(Y)}$ using the atmospheric calibration curve (e.g.,
92 Reimer et al., 2013).

93 As an example, Bondevik et al. (1999) studied a sediment archive recovered on the coast of the
94 Norwegian Sea western Norway. In the slice of sediment (609-611 cm from core top), authors
95 found an articulated shell of *Mytilus edulis* and an assemblage of fragile terrestrial plant material.
96 Here, the sediment slice represents the event Y corresponding to the sediment deposition of *a*
97 *priori* unknown calendar year θ . The ^{14}C ages of the articulated shell and of the terrestrial plant
98 material reflect the ^{14}C ages derived from the reservoir (coastal Norwegian Sea;
99 $\rho_{Norwegian\ Sea}(Y) = 11565 \pm 45$ ^{14}C yr BP) and of the contemporaneous atmosphere ($\rho_{atm}(Y) =$
100 11065 ± 60 ^{14}C yr BP), respectively. According to equation (2) and (3), at the calendar time of
101 the sediment layer deposition (event Y), the ^{14}C reservoir age offset in the costal Norwegian Sea
102 was $d^{14}R_{Norwegian\ sea}(Y) = 500 \pm 75$ ^{14}C years. Finally calibrating the atmosphere-derived
103 ^{14}C age using Intcal13 calibration curve provides the calendar age of event Y : $\theta = 12925 \pm 70$
104 cal. a. BP.

105 However, in this approach both samples are mutually allochthonous. In other words, the terrestrial
106 plant material has been inevitably transported before being embedded with the shell in the
107 sediment. Thus, it is certain that the plant material ceased to incorporated radiocarbon at an event
108 Y^* which occurred earlier than event Y reflecting the sediment deposition. Thus, the calculated
109 ^{14}C reservoir age offset is a more or less faithful estimation of the actual one depending on the
110 fact that event Y^* is close or not (through calendar time) to event Y . Nevertheless, by carefully
111 selecting the dated atmospheric and reservoir-derived objects (fragile well preserved leaves, and

112 articulated shells for example), it might be possible to obtain a close estimation of the actual ^{14}C
113 reservoir age offset value (e.g. Bondevik et al., 1999, 2006).

114 Another way to proceed is to take advantage of the virtually instantaneous deposition of volcanic
115 ash (tephra), over wide onshore and offshore areas. In such cases, the eruption and associated
116 tephra deposition in a sedimentary environment represent event Y . If it has been possible to
117 determine from which eruption the tephra has been generated (usually owing to geochemical
118 measurements carried on the tephra shards), and meaning the fact that this specific eruption has
119 been ^{14}C -dated onshore using terrestrial remains, thus the atmosphere-derived ^{14}C age of event Y
120 is known. Then, measuring the ^{14}C age of some material that formed in the reservoir and
121 retrieved in the tephra layer (e.g. foraminifera for oceanic sediment cores) makes it possible to
122 calculate the reservoir age offset. This technique is now more commonly used (e.g. Kwiecien et
123 al., 2008; Siani et al., 2001, 2013; Southon et al., 2013) but has some limitations mainly linked to
124 stratigraphic uncertainties (e.g. bioturbation processes; see Ascough et al., 2005; Bard et al.,
125 1994).

126 Note that equation (3) applies when paired ^{14}C dates are assumed to be synchronous. However,
127 when dealing with multiple pairs from the same sediment layer, often the case in archeological
128 contexts, the synchronous assumption may not apply. As such, more sophisticated approaches
129 involving Markov chain Monte Carlo sampling are required to explicitly incorporate uncertainty
130 in the temporal relationships among paired samples (Jones and Nicholls, 2001; Jones et al., 2007;
131 Bronk Ramsey, 2008, 2009a).

132

133 ***2.2. Reservoir age offset calculation based on a pair of ^{14}C age and perfectly known calendar***
134 ***age***

135 Another approach is to know *a priori* the actual calendar age θ of event Y and to use the
136 atmospheric calibration curve to derive the corresponding atmospheric ^{14}C age. This is
137 particularly easy when dealing with pre-bomb and historical samples, i.e. for samples for which
138 there is no uncertainty on θ .

139 For example, Siani et al. (2000) analyzed a mollusk shell from the collection of a museum. This
140 mollusk was alive when it had been sampled (i.e. event Y) in the Black Sea (i.e. the reservoir) in
141 50 BP [i.e. *anno domini* AD 1900]. There is no uncertainty associated to θ . This mollusk yielded
142 a radiocarbon age $\rho_{Black\ Sea}(Y)$ of 545 ± 40 ^{14}C yrs BP. In the calendar year 50 cal. BP, the
143 Intcal13 atmospheric calibration curve gives a ^{14}C age (i.e. $\rho_{atm}(Y)$) of 71 ± 7 ^{14}C year BP.
144 According to equation (2) and (3), the ^{14}C reservoir age offset in the Black Sea in 50 BP [i.e.
145 $d^{14}R_{Black\ sea}(Y)$] was of 474 ± 41 ^{14}C yr.

146 Although this approach can be applied to coral annual growth bands (e.g. Druffel et al., 2001), it
147 is more generally used for museum collection samples (e.g. Siani et al., 2000; Tisnerat et al.,
148 2010). The main limitation comes from the fact that collections have historical and scientific
149 significance. Samples from museum collection may not always be available for destructive
150 radiocarbon measurements. Furthermore few museum collections exist from prior to ca. AD
151 1700, limiting the temporal range. As well, these collections do not cover all the Earth's areas
152 limiting the spatial range of reservoir age offset reconstruction. Finally, sometimes the
153 information related to the date of entry in the collection may not match the year of death of the
154 samples (for further information regarding limitations, see Ascough et al., 2005).

155

156 **2.3. Reservoir age ^{14}C offset calculation based on a pair of ^{14}C age and weakly known**
157 **calendar age**

158 Things are more complicated when the calendar age θ for event Y is weakly known, i.e. that an
159 uncertainty σ_θ is associated to θ . This arises when the calendar age was obtained from scientific
160 measurements which could have been achieved through uranium-thorium dating for corals or
161 speleothems (e.g. Durand et al., 2013; Southon et al., 2012) or by cross-matching between a
162 sedimentary archive and a series of reference independently dated over the calendar time scale T
163 (Bard et al., 2013; Heaton et al., 2013; Soulet et al., 2011a).

164 In this case for which, event Y has been dated to $\theta \pm \sigma_\theta$ in the calendar time space T , we would
165 like to “uncalibrate” calendar age θ using the atmospheric calibration curve to obtain the
166 corresponding atmosphere-derived ^{14}C age. A way to proceed would be to invert the axis of the
167 calibration curve and to apply the regular calibration process. However, this is impossible since
168 the calibration curve is built so that the ^{14}C time scale R function is a single valued continuum in
169 the calendar time scale T but not vice-versa. Thus to get access to the atmospheric-derived ^{14}C
170 age associated to event Y dated to $\theta \pm \sigma_\theta$, we propose to calibrate each ^{14}C age r of the ^{14}C time
171 scale R and to evaluate the closeness of each resulting calibrated age distribution to the
172 distribution of calendar age θ (**Fig. 1**).

173 In this scheme, the probability distribution of the measured calendar age for event Y given any
174 calendar age t from the calendar time scale T can be represented by a normal distribution
175 evaluated at t and centered on θ with a standard deviation σ_θ :

176
$$p(Y|t) \sim N(t; \theta, \sigma_\theta) \tag{4}$$

177 This can be written as:

178
$$p(Y|t) = \frac{1}{\sigma_\theta \sqrt{2\pi}} \exp\left(-\frac{(t-\theta)^2}{2\sigma_\theta^2}\right) \quad (5)$$

179 This quantity evaluate the closeness between the occurrence of event Y and any time through the
 180 calendar age scale T . Additionally, we have information about how the ^{14}C and calendar time
 181 scales are related. The information comes from the atmospheric calibration curve which links the
 182 ^{14}C time scale R to the calendar time scale T . For any time t from the calendar time scale T , the
 183 atmospheric calibration curve is defined as $\rho(t) \pm \sigma(t)$ on the radiocarbon time scale R . Here
 184 $\rho(t)$ is the ^{14}C age of the atmosphere at calendar time t . For any age r from the ^{14}C time scale R ,
 185 this information is normally taken to be:

186
$$p(r|t) \sim N(r; \rho(t), \sigma(t)) \quad (6)$$

187 This can be written as:

188
$$p(r|t) = \frac{1}{\sigma(t)\sqrt{2\pi}} \exp\left(-\frac{(r-\rho(t))^2}{2\sigma^2(t)}\right) \quad (7)$$

189 Now, let's assume the following Bayesian network: $Y \leftrightarrow T \rightarrow R$. In this network, the calendar
 190 time scale T is our hypothesis (or *prior*). Furthermore, we know that the radiocarbon time scale
 191 R depends upon the calendar time scale T (i.e. the calibration curve or the *model*) and we want to
 192 evaluate the closeness (or *likelihood*) between the calendar age measurement for event Y (our
 193 *observation*) and the calibration curve. According to the network and Bayes' theorem, we write:

194
$$p(Y|t, r) \propto p(Y|t) \cdot p(r|t) \cdot p(t) \quad (8)$$

195 The symbol \propto denotes proportionality. The *prior* along the calendar time scale T is taken as
 196 uniform:

197
$$p(t) \sim U(-\infty, +\infty) \tag{9}$$

198 and is thus equal to a constant:

199
$$p(t) = \text{constant} \tag{10}$$

200 Thus according to equations (9) and (10), we say:

201
$$p(Y|t, r) \propto p(Y|t) \cdot p(r|t) \tag{11}$$

202 By substituting equations (5) and (7) in equation (11), we can rewrite as follows:

203
$$p(Y|t, r) \propto \frac{1}{\sigma_\theta \cdot \sigma(t)} \exp\left(-\frac{(t-\theta)^2}{2\sigma_\theta^2}\right) \cdot \exp\left(-\frac{(r-\rho(t))^2}{2\sigma^2(t)}\right) \tag{12}$$

204 We now can integrate out parameter t :

205
$$p(Y|r) \propto \int p(Y|t) \cdot p(r|t) \cdot dt \tag{13}$$

206 The “uncalibrated” ^{14}C age (or *posterior*) defines the probability of obtaining a given ^{14}C age r
 207 from the radiocarbon time scale R given the event Y . From Bayes’ theorem, the *posterior* is
 208 given by:

209
$$p(r|Y) \propto p(Y|r) \cdot p(r) \tag{14}$$

210 The *prior* along the radiocarbon time scale R is taken uniform. Thus $p(r)$ is constant and the
 211 probability distribution of the “uncalibrated” ^{14}C age (*posterior*) is the same as that for the
 212 *likelihood*:

213
$$p(r|Y) \propto p(Y|r) \tag{15}$$

214 Finally, to obtain the probability distribution of the atmospheric-derived ^{14}C age along the ^{14}C
 215 time scale R (i.e. the “uncalibrated” ^{14}C age) given the single event Y for which we know the
 216 calendar measurement $\theta \pm \sigma_\theta$, we normalize to 1. This gives:

$$217 \quad p(r|Y)_{atm} = \frac{p(r|Y)}{\int p(r|Y) \cdot dr} \quad (16)$$

218 Here the denominator is the normalizing constant. The subscript “atm” on the left term of
 219 equation (16) stands to emphasize that this probability distribution is our atmospheric-derived
 220 ^{14}C age. At that step, we have “uncalibrated” our calendar age. Remember that event Y is
 221 characterized by both its calendar age and the ^{14}C age of the reservoir. We can write:

$$222 \quad \rho_{atm}(Y) = p(r|Y)_{atm} \quad \text{and} \quad \rho_{res}(Y) = p(r|Y)_{res} \quad (17)$$

223 Now, according to equation (3), to find the probability distribution of the reservoir age offset
 224 which is $p(d^{14}R|Y)$, we have to subtract both quantities. Since both ^{14}C age distributions are
 225 independent, we use the convolution product:

$$226 \quad p(d^{14}R|Y) = p(r|Y)_{res} * (-\mathbb{1}_R \cdot p(r|Y)_{atm}) \quad (18)$$

227 Here, $-\mathbb{1}_R$ means that we multiply by -1 the atmospheric-derived ^{14}C age along the ^{14}C time
 228 scale R before summing both probability distributions through the convolution product, and
 229 finally:

$$230 \quad d^{14}R(Y) = p(d^{14}R|Y) \quad (19)$$

231 The *uncalibration-convolution process* fully propagates uncertainties linked to the reservoir-
 232 derived ^{14}C age and the calendar age of event Y , as well as the calibration curve wiggles and

233 uncertainties. **Fig. 1** shows that the both the uncalibrated ^{14}C age and the resulting reservoir age
234 offset are not necessarily Gaussian in shape.

235 The *uncalibration-convolution process* developed here does not take into account any
236 sedimentary ordering constraints that are available when dealing with high-resolution records of
237 calendar observations. Ordering constraints can be incorporated in the calculations of reservoir
238 age offset using some recent developments of the program OxCal (Bronk Ramsey et al., 2012;
239 Bronk Ramsey and Lee, 2013).

240 ***2.4. The “ResAge” package: open-source codes for reservoir age offset calculations***

241 Here, three codes for reservoir age offset calculation performing the above detailed three
242 methodologies are provided (*ResAge* package). From data inputs (depending on the chosen
243 approach), the codes provide the reservoir age ^{14}C offset outputs as well as some optional data.

244 Codes from the *ResAge* package have been written in the open-source environment R (R
245 Development Core Team, 2014). R is freely downloadable at <http://www.r-project.org> for
246 Windows, Mac and Linux. The codes make use of a command-window. The number of
247 commands to be typed is extremely limited making very easy the use of these codes. Moreover,
248 basics in R are relatively easy to learn, and the use of R in paleo-research has been growing
249 recently (Blaauw, 2010; Blaauw and Christen, 2005, 2011; Haslett and Parnell, 2008; Heegaard
250 et al., 2005). A manual containing information for installing and using the codes is also provided
251 (see supplementary information).

252 Briefly, code “*rad2.r*” (say rad squared) is designed to calculate reservoir age offset when both
253 the reservoir-derived and atmosphere-derived ^{14}C ages are known (see section 2.1). It returns a
254 .csv file as output. Upon the user’s decision, the atmospheric-derived ^{14}C ages can be calibrated.

255 An additional .csv file containing the calibrated density probabilities can be used to draw them.
256 A .txt file reports the unnormalized highest posterior probability as the confidence interval
257 specified by the user (see Blaauw, 2010).

258 Code “*colyear.r*” is designed for pairs of reservoir-derived ^{14}C age and perfectly known calendar
259 year (museum collection samples, coral annual band growths; see section 2.2). The code looks
260 up the calendar year in the atmospheric calibration curve, returns the corresponding atmosphere-
261 derives ^{14}C age and calculate the ^{14}C reservoir age offset. A .csv file is generated with all
262 information.

263 Code “*radcal.r*” is designed for pairs of reservoir-derived ^{14}C age and weakly-known calendar
264 age (e.g. ^{14}C and U/Th dating of corals and speleothem; see section 2.3). The calendar ages are
265 “uncalibrated” to obtain the corresponding atmosphere-derived ^{14}C age following the above
266 detailed procedure and ^{14}C reservoir age offsets are calculated through a convolution product.
267 Similar to Bronk Ramsey (2009b) and Blaauw (2010), calculations are performed in reference to
268 the ratio $F^{14}\text{C}$ (Reimer et al., 2004) instead of the ^{14}C age (Stuiver and Polach, 1977), allowing
269 for the best representation of all the ^{14}C uncertainties. Code returns a .csv file containing the ^{14}C
270 reservoir age offset density probabilities that can be used to draw them. A .txt file reports the
271 highest posterior probability as the confidence interval specified by the user. Upon user’s request
272 the same information and files can be obtained for the “uncalibrated” atmospheric ^{14}C ages.

273

274 **3. A case study**

275 Speleothems are promising archives to reconstruct past changes in the atmospheric ^{14}C
276 concentration. In 2013, three of these archives have been included for the first time in the
277 Intcal13 dataset in order to extend and refine the latest release of the internationally ratified

278 atmospheric calibration curve (Intcal13; Reimer et al., 2013). Speleothems are secondary mineral
279 deposits that precipitate from drip water in caves. They are mainly composed of calcite,
280 aragonite and polymorphs of calcium carbonate and are considered as closed systems and thus
281 suitable for ^{14}C measurements. Uranium from the groundwater is co-precipitated in calcite and
282 aragonite with negligible thorium, making possible the use of U-Th dating methods and thus
283 providing an independent calendar time scale. Accordingly, the three speleothem implemented in
284 the Intcal13 dataset – two from the Bahamas (Beck et al., 2001; Hoffman et al., 2010) and one
285 from China (Southon et al., 2012) – are dated through pairs of ^{14}C and U-Th ages. However, in
286 the case of speleothems, obtained raw ^{14}C ages must be corrected for Dead Carbon Fraction
287 (DCF) in order to estimate the “atmospheric equivalent” ^{14}C concentration. Indeed, DCF is the
288 reservoir age offset between the speleothem and the atmosphere. DCF arises from the
289 incorporation of a portion of ^{14}C -free inorganic carbon in the speleothem at the time of carbonate
290 calcium precipitation (e.g. Fohlmeister et al., 2011; Genty and Massault, 1997). This portion of
291 “dead” carbon is mainly due to dissolution of ^{14}C -free carbonate rocks overlying the cave.

292 As described in *Selection and Treatment of Data for ^{14}C Calibration* (Reimer et al., 2013b), DCF
293 is estimated by analyzing a section of the speleothem that overlaps with the tree-ring-based
294 section of the calibration curve (0-14,000 cal. a. BP in the Intcal13 latest release). The mean ^{14}C
295 offset between the ^{14}C age of the speleothem and the tree-ring-based portion of the calibration
296 curve is then use as the DCF. An uncertainty term is then introduced. It quadratically takes into
297 account the standard deviation of the individually calculated DCFs and the combined error of the
298 ^{14}C measurement and of the inferred atmospheric ^{14}C related to the calibration curve (Reimer et
299 al., 2013a, 2013b; Southon et al., 2012). In this approach, uncertainty in the U/Th ages and the
300 wiggles of the calibration curve are not taken into account.

301 Here, the DCFs of the three speleothem-datasets [Hulu Cave H82 speleothem (Southon et al.,
302 2012) and Bahamas speleothems GP89-24-1 and GP89-25-3 (Beck et al., 2001; Hoffmann et al.,
303 2010, respectively)] for data overlapping the tree-ring based calibration curve are calculated
304 applying the methodology detailed in section 2.3 through the use of the function *radcal*
305 described in section 2.4).

306 Depending upon the number of data to be processed and on the uncertainty linked to the calendar
307 U/Th age, calculations take up few seconds on a modern PC: ~5 sec for the 80 Hulu Cave data
308 (mean $\sigma_{U/Th}$ of 30 yrs), ~7 sec for the 63 GP89-24-1 data (mean $\sigma_{U/Th}$ of 40 yrs) and ~20 sec for
309 the 116 GP89-25-3 data (mean $\sigma_{U/Th}$ of 45 yrs).

310 Calculated DCFs for Hulu Cave H82 show no noticeable structures with limited variability with
311 time – 95%-confidence interval of 308 to 615 ^{14}C years with a mode (highest probability) at 433
312 ^{14}C years (**Fig. 2**). DCF variability for both Bahamas speleothem is considerably larger - 95%-
313 confidence interval 1045 to 2099 ^{14}C years with a mode at 1405 ^{14}C years for GP89-24-1
314 speleothem (Beck et al., 2001) and 95%-confidence interval 1527 to 2755 ^{14}C years with a mode
315 at 2124 ^{14}C years for GP89-25-3 speleothem (Hoffmann et al., 2010) (**Fig. 2**). Perhaps, a
316 problematic feature is the marked structure seen in GP89-25-3 speleothem (Hoffmann et al.,
317 2010) showing fast and high-amplitude changes in the DCF. As an example, between *c.* 12,200
318 and 11,900 cal. a. BP, DCF decreases by 1200 ^{14}C years. GP89-25-3 speleothem data are
319 invaluable data that are currently used as input data to reconstruct the atmospheric ^{14}C calibration
320 curve (Reimer et al., 2013a, 2013b). However, even corrected for a wide average DCF, such a
321 structure occurring in older part of the speleothem record may introduce uncertainties by an
322 order of 1000 cal. years for the older portion of the atmospheric ^{14}C calibration curve. Most of
323 all, further developing our understanding of the controls on the incorporation of dead carbon in

324 speleothems (e.g. Fohlmeister et al., 2011; Noronha et al., 2014; Reimer et al., 2013b) and in a
325 general manner on the reservoir age offset of the marine data implemented in the ^{14}C calibration
326 curve are both of primary interest (Reimer et al., 2013b).

327

328 **4. Conclusions**

329 Proper calculation of reservoir age offset is of primary interest since their reconstruction through
330 time tells a lot about the changes in the regional to global-scale carbon cycle with impacts on our
331 understanding of the Earth climate. In particular, proper regional reconstruction of reservoir age
332 offsets is important to build regional calibration curve. Regional calibration curves may be
333 suitable for very specific basins (e.g. Black Sea, Caspian Sea) for which reservoir offsets are
334 supposed to have greatly varied with time and for which assessing reliable sediment archive
335 chronologies is challenging (e.g. Kwiecien et al., 2008; Soulet et al., 2011a, 2011b). Regional
336 surface ocean calibration curves are also needed to better constrain changes in the oceanic
337 ventilation age through the projection age methods (Lund, 2013). R codes and the innovative
338 calculation method based on pairs of ^{14}C age and calendar ages presented here would represent
339 another step to study reservoir age offset evolution with more scrutiny. Future improvements and
340 development aiming at properly calculating the reservoir age offset evolution with time would be
341 useful. Finally, the R codes composing the *ResAge* package can be understood relatively easily.
342 Interested users can open and adapt the “black box”.

343

344 **References:**

345 Ascough, P., Cook, G., Dugmore, A., 2005. Methodological approaches to determining the marine
346 radiocarbon reservoir effect. *Progress in Physical Geography*, 29(4), 532-547.

347 Bard, E., Arnold, M., Mangerud, J., Paterne, M., Labeyrie, L., Duprat, J., Mélières, M.-A., Sønstegaard,
348 E., Duplessy, J. C., 1994. The North Atlantic atmosphere-sea surface ^{14}C gradient during the
349 Younger Dryas climatic event. *Earth and Planetary Science Letters*, 126(4), 275-287.

350 Bard, E., Ménot, G., Rostek, F., Licari, L., Böning, P., Edwards, R.L., Cheng, H., Wang, Y., Heaton, T.J.,
351 2013. Radiocarbon calibration/comparison records based on marine sediments from the Pakistan
352 and Iberian margins. *Radiocarbon*, 55(4), 1999-2019.

353 Beck, J.W., Richards, D.A., Lawrence, R., Silverman, B.W., Smart, P.L., Donahue, D.J., Herrera-
354 Osterheld, S., Burr, G.S., Calsoyas, L., Jull, A.J.T., Biddulph, D., 2001. Extremely large
355 variations of atmospheric ^{14}C concentration during the last glacial period. *Science*, 292(5526),
356 2453-2458.

357 Blaauw, M., 2010. Methods and code for 'classical' age-modelling of radiocarbon sequences. *Quaternary*
358 *Geochronology*, 5(5), 512-518.

359 Blaauw, M., Christen, J.A., 2005. Radiocarbon peat chronologies and environmental change. *Applied*
360 *Statistics* 54, 805-816.

361 Blaauw, M., Christen, J.A., 2011. Flexible paleoclimate age-depth models using an autoregressive gamma
362 process. *Bayesian Analysis*, 6(3), 457-474.

363 Bondevik, S., Birks, H.H., Gulliksen, S., Mangerud, J., 1999. Late Weichselian Marine ^{14}C Reservoir
364 Ages at the Western Coast of Norway. *Quaternary Research*, 52(1), 104-114.

365 Bondevik, S., Mangerud, J., Birks, H.H., Gulliksen, S., Reimer, P., 2006. Changes in North Atlantic
366 radiocarbon reservoir ages during the Allerød and Younger Dryas. *Science*, 312(5779), 1514-
367 1517.

368 Bronk Ramsey, C., 2008. Deposition models for chronological records. *Quaternary Science Reviews*, 27,
369 42-60.

370 Bronk Ramsey, C., 2009a. Dealing with outliers and offsets in radiocarbon dating. *Radiocarbon*, 51(3),
371 1023-1045.

372 Bronk Ramsey, C., 2009b. Bayesian analysis of radiocarbon dates. *Radiocarbon*, 51(1), 337-360.

373 Bronk Ramsey, C., Lee, S., 2013. Recent and planned developments of the program OxCal. *Radiocarbon*,
374 55(2-3), 720-730.

375 Ramsey, C.B., Staff, R.A., Bryant, C.L., Brock, F., Kitagawa, H., van der Plicht, J., Scholaut, G.,
376 Marshall, M.H., Brauer, A., Lamb, H.F., Payne, R.L., Tarasov, P.E., Haraguchi, T., Gotanda, K.,
377 Yonenobu, H., Yokoyama, Y., Tada, R., Nakagawa, T. (2012). A complete terrestrial
378 radiocarbon record for 11.2 to 52.8 kyr BP. *Science*, 338(6105), 370-374.

379 Druffel, E.R., Griffin, S., Guilderson, T.P., Kashgarian, M., Southon, J., Schrag, D.P., 2001. Changes of
380 subtropical North Pacific radiocarbon and correlation with climate variability. *Radiocarbon*, 43(1),
381 15-25.

382 Druffel, E.R., Robinson, L.F., Griffin, S., Halley, R.B., Southon, J.R., Adkins, J.F., 2008. Low reservoir
383 ages for the surface ocean from mid-Holocene Florida corals. *Paleoceanography*, 23(2), PA2209.
384 doi: 10.1029/2007PA001527.

385 Durand, N., Deschamps, P., Bard, E., Hamelin, B., Camoin, G., Thomas, A.L., Henderson, G.H.,
386 Yokoyama, Y., Matsuzaki, H., 2013. Comparison of ^{14}C and U-Th ages in corals from IODP
387 #310 cores offshore Tahiti. *Radiocarbon*, 55(4), 1947-1974.

388 Fohlmeister, J., Kromer, B., Mangini, A., 2011. The influence of soil organic matter age spectrum on the
389 reconstruction of atmospheric ^{14}C levels via stalagmites. *Radiocarbon*, 53(1), 99-115.

390 Gentil, D., Massault, M., 1997. Bomb ^{14}C recorded in laminated speleothems: calculation of dead carbon
391 proportion. *Radiocarbon* 33(1):33-48.

392 Hall, B.L., Henderson, G.M., Baroni, C., Kellogg, T.B., 2010. Constant Holocene Southern-Ocean ^{14}C
393 reservoir ages and ice-shelf flow rates. *Earth and Planetary Science Letters* 296(1), 115-123.

394 Haslett, J., Parnell, A., 2008. A simple monotone process with application to radiocarbon-dated depth
395 chronologies. *Applied Statistics* 57, 1-20.

396 Heaton, T.J., Bard, E., and Hughen, K.A., 2013. Elastic Tie-Pointing—Transferring Chronologies
397 between Records Via a Gaussian Process. *Radiocarbon* 55(4), 1975-1997.

398 Heegaard, E., Birks, H.J.B., Telford, R.J., 2005. Relationships between calibrated ages and depth in
399 stratigraphical sequences: an estimation procedure by mixed effect regression. *The Holocene* 15,
400 1-7.

401 Hoffmann, D.L., Beck, J.W., Richards, D.A., Smart, P.L., Singarayer, J.S., Ketchmark, T. Hawkesworth,
402 C.J., 2010. Towards radiocarbon calibration beyond 28ka using speleothems from the Bahamas.
403 Earth and Planetary Science Letters, 289(1), 1-10.

404 Hogg, A. G., Hua, Q., Blackwell, P. G., Niu, M., Buck, C. E., Guilderson, T. P., Heaton, T. J., Palmer, J.
405 G., Reimer, P. J., Reimer, R. W., Turney, C. S. M., and Zimmerman, S. R. H., 2013. SHCal13
406 Southern Hemisphere calibration, 0–50,000 years cal BP. Radiocarbon, 55(4), 1889-1903.

407 Jones M, Nicholls G., 2001. Reservoir offset models for radiocarbon calibration. Radiocarbon, 43(1),
408 119–24.

409 Jones M, Petchey F, Green R, Sheppard P, Phelan M., 2007. The marine ΔR for Nenumbo (Solomon
410 Islands): a case studying calculating reservoir offsets from paired sample data. Radiocarbon,
411 49(1), 95–102.

412 Jull, A. J., Burr, G.S., Hodgins, G.W., 2013. Radiocarbon dating, reservoir effects, and calibration.
413 Quaternary International 299, 64-71.

414 Kwiecien, O., Arz, H.W., Lamy, F., Wulf, S., Bahr, A., Rohl, U., Haug, G.H., 2008. Estimated reservoir
415 ages of the Black Sea since the last glacial. Radiocarbon, 50(1), 99.

416 Lund, D.C., 2013. Deep Pacific ventilation ages during the last deglaciation: Evaluating the influence of
417 diffusive mixing and source region reservoir age. Earth and Planetary Science Letters, 381, 52-
418 62.

419 Noronha, A.L., Johnson, K.R., Hu, C., Ruan, J., Southon, J.R., Ferguson, J.E., 2014. Assessing influences
420 on speleothem dead carbon variability over the Holocene: Implications for speleothem-based
421 radiocarbon calibration. Earth and Planetary Science Letters, 394, 20-29.

422 R Core Team, 2014. R: A Language and Environment for Statistical Computing. R Foundation for
423 Statistical Computing, <http://www.R-project.org>.

424 Reimer, P.J., Bard, E., Bayliss, A., Beck, J.W., Blackwell, P.G., Bronk Ramsey, C., Buck, C.E., Cheng,
425 H., Edwards, R.L., Friedrich, M., Grootes, P.M., Guilderson, T.P., Haflidason, H., Hajdas, I.,
426 Hatté, C., Heaton, T.J., Hoffmann, D.L., Hogg, A.G., Hughen, K.A., Kaiser, K.F., Kromer, B.,
427 Manning, S.W., Niu, M., Reimer, R.W., Richards, D.A., Scott, E.M., Southon, J.R., Staff, R.A.,
428 Turney, C.S.M., and van der Plicht, J., 2013a. IntCal13 and Marine13 Radiocarbon Age
429 Calibration Curves 0–50,000 Years cal BP. Radiocarbon 55(4), 1869-1887.

430 Reimer, P.J., Bard, E., Bayliss, A., Beck, J.W., Blackwell, P.G., Ramsey, C.B., Brown, D.M., Buck, C.E.,
431 Edwards, R.L., Friedrich, M., Grootes, P.M., Guilderson, T.P., Haflidason, H., Hajdas, I., Hatté,
432 C., Heaton, T.J., Hogg, A.G., Hughen, K.A., Kaiser, K.F., Kromer., B., Manning, S.W., Reimer,
433 R.W., Richards, D.A., Scott, E.M., Southon, J.R., Turney, C.S.M., van der Plicht, J., 2013b.
434 Selection and treatment of data for radiocarbon calibration: an update to the International
435 Calibration (IntCal) criteria. *Radiocarbon*, 55(4), 1923-1945.

436 Reimer, P.J., Brown, T.A., Reimer, R.W., 2004. Discussion: reporting and calibration of post-bomb ¹⁴C
437 data. *Radiocarbon*, 46(3), 1299-1304.

438 Siani, G., Michel, E., De Pol-Holz, R., DeVries, T., Lamy, F., Carel, M., Isguder, G., Dewilde, F.,
439 Lourantou, A., 2013. Carbon isotope records reveal precise timing of enhanced Southern Ocean
440 upwelling during the last deglaciation. *Nature communications*, 4. doi: 10.1038/ncomms3758.

441 Siani, G., Paterne, M., Arnold, M., Bard, E., Mativier, B., Tisnerat, N., Bassinot, F., 2000. Radiocarbon
442 reservoir ages in the Mediterranean Sea and Black Sea. *Radiocarbon*, 42(2), 271-280.

443 Siani, G., Paterne, M., Michel, E., Sulpizio, R., Sbrana, A., Arnold, M., Haddad, G., 2001. Mediterranean
444 Sea surface radiocarbon reservoir age changes since the last glacial maximum. *Science*,
445 294(5548), 1917-1920.

446 Soulet, G., Ménot, G., Garreta, V., Rostek, F., Zaragosi, S., Lericolais, G., Bard, E., 2011a. Black Sea
447 "Lake" reservoir age evolution since the Last Glacial - Hydrologic and climatic implications.
448 *Earth and Planetary Science Letters* 308, 245-258.

449 Soulet, G., Ménot, G., Lericolais, G., Bard, E., 2011b. A revised calendar age for the last reconnection of
450 the Black Sea to the global ocean. *Quaternary Science Reviews*, 30(9), 1019-1026.

451 Southon, J., Mohtadi, M., De Pol-Holz, R., 2013. Planktonic foram dates from the Indonesian Arc: marine
452 ¹⁴C reservoir ages and a mythical AD 535 eruption of Krakatau. *Radiocarbon*, 55(2-3), 1164-
453 1172.

454 Southon, J., Noronha, A.L., Cheng, H., Edwards, R.L., Wang, Y., 2012. A high-resolution record of
455 atmospheric ¹⁴C based on Hulu Cave speleothem H82. *Quaternary Science Reviews* 33, 32-41.

456 Southon, J., Noronha, A.L., Cheng, H., Edwards, R.L., Wang, Y., 2012. A high-resolution record of
457 atmospheric ¹⁴C based on Hulu Cave speleothem H82. *Quaternary Science Reviews*, 33, 32-41.

458 Stuiver, M., Polach, H.A., 1977. Discussion: reporting of ¹⁴C data. *Radiocarbon*, 19(3), 355-363.

459 Thornalley, D.J.R., Barker, S., Broecker, W.S., Elderfield, H., McCave, I.N., 2011. The Deglacial
460 Evolution of North Atlantic Deep Convection. *Science* 331(6014), 202-205.

461 Tisnérat-Laborde, N., Paterne, M., Métivier, B., Arnold, M., Yiou, P., Blamart, D., Raynaud, S., 2010.
462 Variability of the northeast Atlantic sea surface $\Delta^{14}\text{C}$ and marine reservoir age and the North
463 Atlantic Oscillation (NAO). *Quaternary Science Reviews*, 29(19), 2633-2646.

464

465 **Acknowledgements:** G.S. acknowledges the Postdoctoral Scholar Program at the Woods
466 Hole Oceanographic Institution (WHOI), with funding provided by the National Ocean Sciences
467 Accelerator Mass Spectrometry Facility (NOSAMS). G.S. warmly thanks Beatrice Tomasi,
468 William J. Jenkins, Steven R. Beaupré, Ann P. McNichol, Kirstyn Fornace, Liviu Giosan and
469 Valier Galy for fruitful discussions and support.

470

471

472

473 **Figure captions:**

474 **Fig. 1:** Calculation of a ^{14}C reservoir age offset based on a pair of reservoir-derived ^{14}C date of
475 9200 ± 30 ^{14}C yr BP (grey Gaussian probability density function [pdf] on the radiocarbon time
476 axis) and calendar date of 9550 ± 150 cal. yr BP (light green Gaussian pdf on the calendar time
477 axis). A: “Uncalibration” of the calendar date following the methodology detailed in section 2.3.
478 The resulting “uncalibrated” age (light green multimodal pdf on the radiocarbon time axis)
479 corresponds to the atmosphere-derived ^{14}C age involved in the ^{14}C reservoir age offset
480 calculation. Highest posterior density ranges (black bars) of the “uncalibrated” age are 8272 –
481 8601 ^{14}C yr BP (probability 43.8%) and 8605 – 8826 ^{14}C yr BP (probability 51.2%). Black curve

482 is the 1σ Intcal13 envelope (Reimer et al., 2013). B: The resulting ^{14}C reservoir age offset
483 (purple pdf) corresponding to the difference between the reservoir-derived ^{14}C age (grey
484 Gaussian pdf in A) and the atmosphere-derived ^{14}C age (light green multimodal pdf in A)
485 through a convolution product. Highest posterior density ranges (black bars) of the ^{14}C reservoir
486 age offset are $362 - 617$ ^{14}C years (probability 51.9%) and $622 - 947$ ^{14}C years (probability
487 43.1%).

488

489 **Fig. 2:** Reconstruction of the changes in the ^{14}C reservoir age offset (i.e. dead carbon fraction,
490 DCF) for the three speleothem data currently included in the Intcal13 database. DCF is
491 calculated for ^{14}C -calendar pairs overlapping the tree-ring based atmospheric calibration curve
492 (Intcal13; Reimer et al., 2013). Yellow and green squares: Bahamas speleothems GP89-25-3
493 (Hoffmann et al., 2010) and GP89-24-1 (Beck et al., 2001), respectively. Blue circles: Chinese
494 Hulu Cave speleothem H82 (Southon et al., 2012). Yellow, green and blue probability density
495 functions (pdf) represent the corresponding full variability in the DCF calculated as the mixture
496 of all the individual DCF pdfs for each set of data: Highest posterior density ranges at 95%
497 (shaded areas) and modes are $1527 - 2755$ ^{14}C years with mode at 2124 ^{14}C years (Bahamas
498 GP89-25-3), $1045 - 2099$ ^{14}C years with mode at 1405 ^{14}C years (Bahamas GP89-24-1) and 308
499 $- 615$ ^{14}C years with mode at 433 ^{14}C years (Chinese Hulu cave H82). All uncertainties
500 characterizing data are given at 95% confidence.

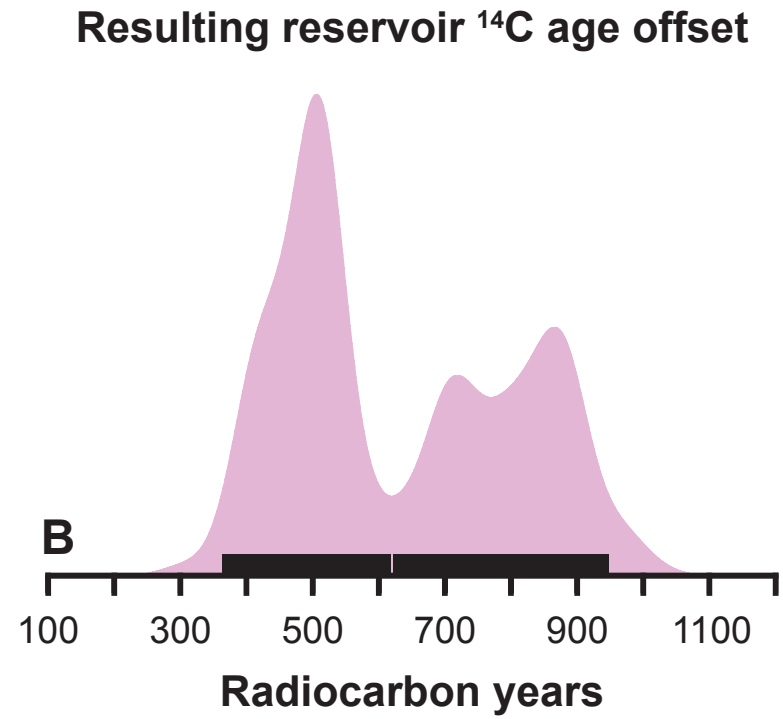
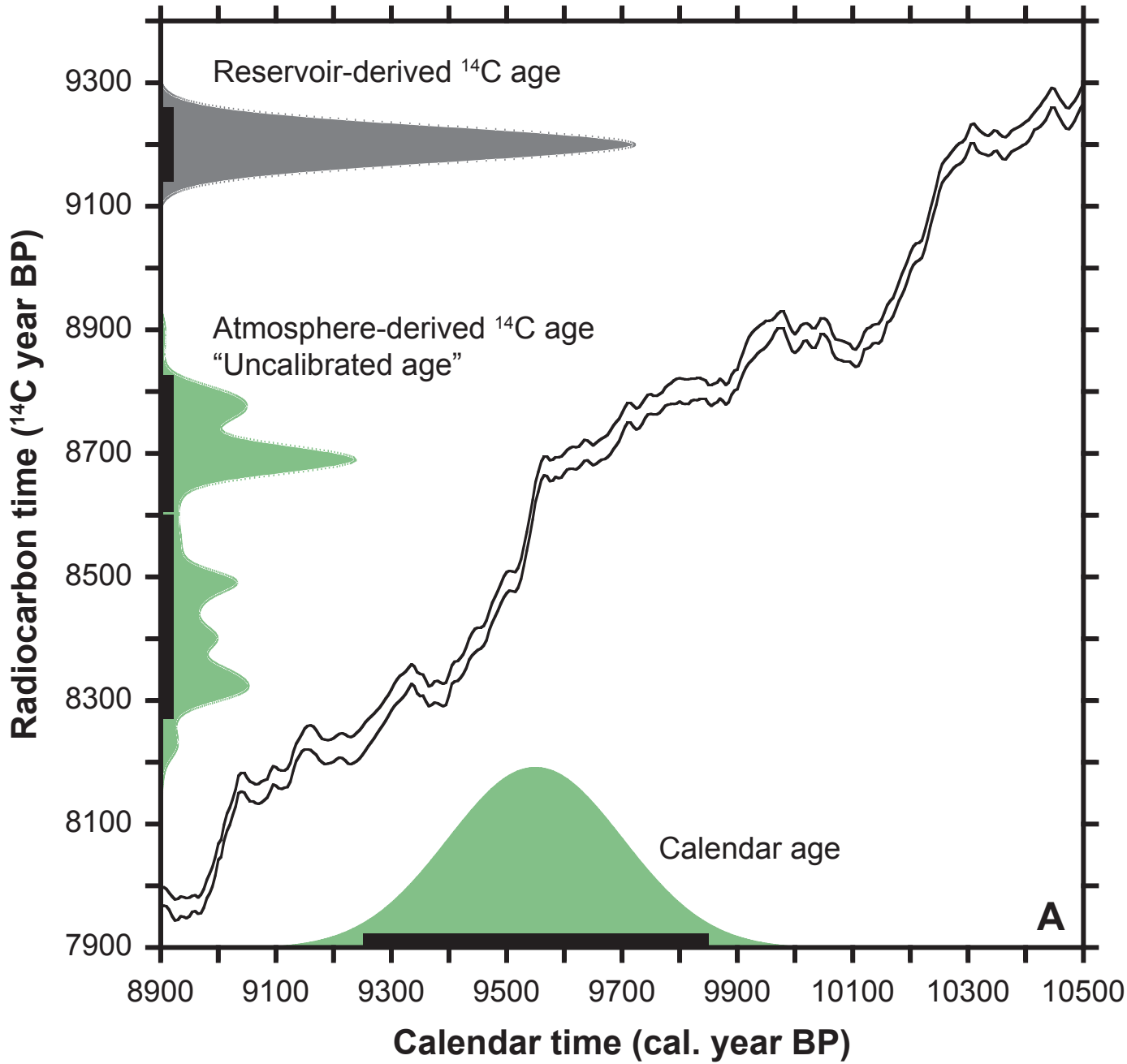


Figure 1.

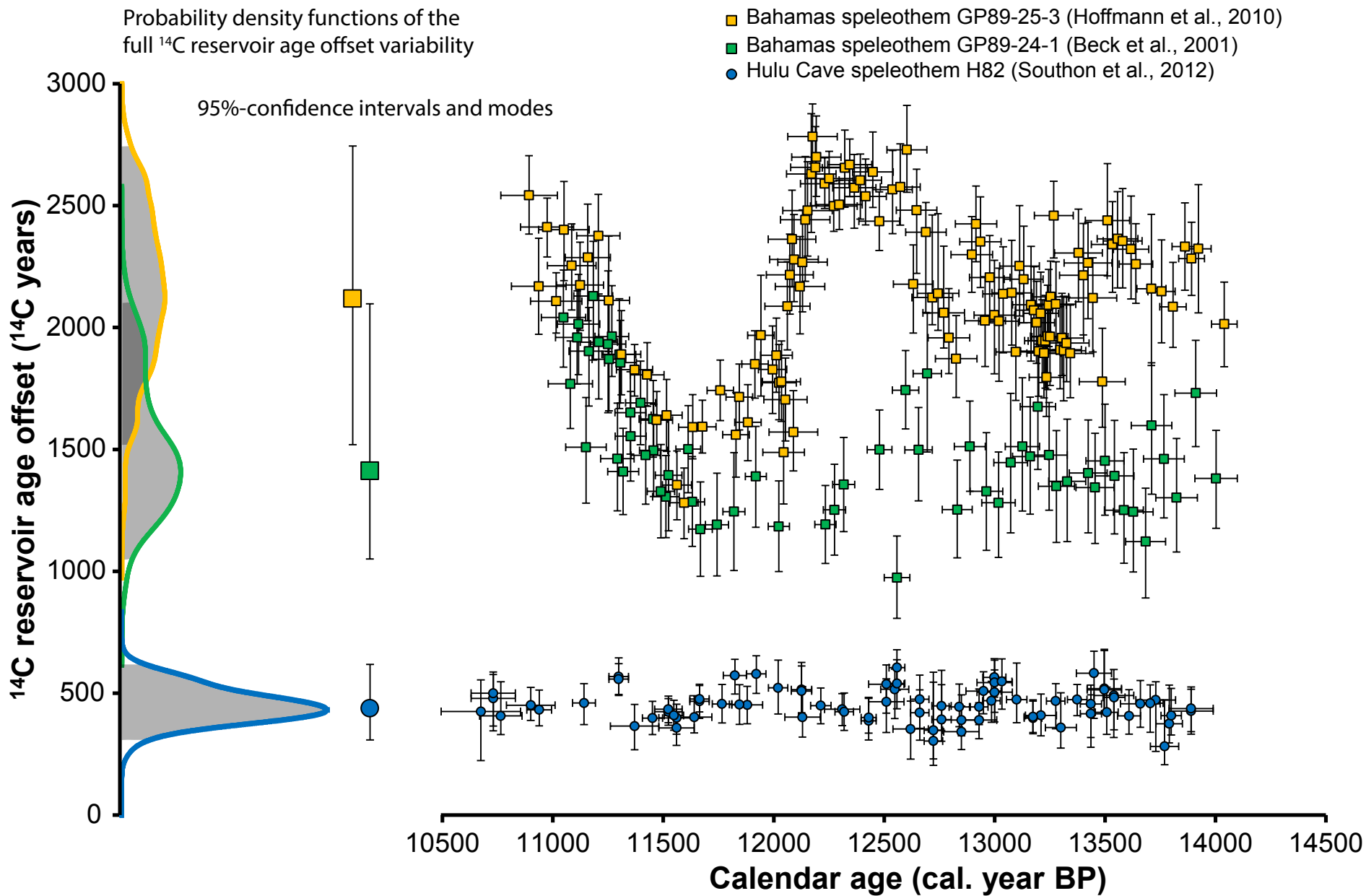


Figure 2.